www.czasopisma.pan.pl PAN POLSKA AKADEMIA NAUK www.journals.pan.pl

Arch. Metall. Mater. **67** (2022), 4, 1227-1234

DOI: https://doi.org/10.24425/amm.2022.141046

NGUYEN QUANG HOC[1*], BUI DUC TINH[1], NGUYEN DUC HIEN[2]

THE MELTING AND THE DEBYE TEMPERATURE OF FOR BCC AND FCC METALS UNDER PRESSURE: A CALCULATION FROM THE STATISTICAL MOMENT METHOD

We build the melting theory and the theory of the Debye temperature for defective and perfect cubic metals mainly based on the statistical moment method. Our theoretical results are applied to metals Ni, Pd and Pt. Our calculations of melting temperatures agree well with experiments and other calculations. Our other calculations are highly reliable.

Keywords: Statistical moment method; defective and perfect cubic metals and Debye temperature

1. Introduction

Studying on the melting of the crystal is a classic problem. Experimental techniques consist of the laser-heating diamond anvil cell (LH DAC) [1] and the shock wave (SW) [2]. Main theories and simulations are the molecular dynamics simulation (MD) [3] and the *ab initio* calculations [4]. However, the experiments do not agree with theoretical results for the melting of some transition metals [5]. At the melting point, many physical quantities such as the atomic volume, the density, the enthalpy, the entropy, etc. have jumps. Although some theoretical researchers tried to solve this problem [6,7], the obtained results are still limited.

Researchers have been interested the melting of metals Ni, Pd and Pt. At 0.1 MPa, The BCC structure of Ni has the lattice constant $a = 3.5328\times10^{-10}$ m and the melting temperature 1728 K at 0,1 MPa. The experimental melting curve of Ni has the constant dT/dP = 33 K/GPa up to 1923K and 6 GPa [8,9]. The melting curve of Ni was experimentally and theoretically determined in [10-12]. The behavior of Ni was studied at room temperature by calculation up to 34 TPa[13]. According to X-ray diffraction study, the FCC structure of Ni is stable at 298K up to 65 GPa [14] and up to 55 GPa for nanocrystalline Ni [15]. The BCC structure of Pd has the lattice constant $a = 3.8902\times10^{-10}$ m and the melting temperature 1827K at 0.1 MPa. The behavior of Pd was studied by X-ray diffraction up to 80 GPa and 298 K [16,17], by calculation [18] and in [19,20]. The FCC structure of Pt has the lattice constant $a = 3.9239\times10^{-10}$ m and the melting temparature 2057 K at 0.1 MPa. The behavior of Pt was studied at melting by calculations [12,21-23]. The melting curve has an initial dT/dP = 42 K/GPa up to 6 GPa and ~2300 K [24]. The melting curve was presented by the equation T(K) = 2057 + $27.2P - 0.1497P^2$, where P is in GPa [25].

In recent years, many simulations and theoretical studies on the influences of factors such as temperature, pressure, atomic number, impurities,... on structural, mechanical; thermodynamic, melting and electrical properties, phase transtions of metals, alloys and polymers have been published [26-37].

In this paper, we present the melting theory and the theory of Debye temperature for cubic metals mainly builded by the statistical moment method (SMM). Our theory is applied to metals Ni, Pd and Pt. We compare and interpret the numerical results obtained.

[1] HANOI NATIONAL UNIVERSITY OF EDUCATION, 136 XUAN THUY, HANOI, VIETNAM
[2] MAC DINH CHI HIGH SCHOOL, CHU PAH DISTRICT, GIA LAI PROVINCE, VIETNAM

* Correspongding author: hocnq@hnue.edu.vn

2. Theoretical model

The Helmholtz free energy of cubic metals is equal to [38,39]

$$\psi = U_0 + \psi_0 + 3N\left\{\frac{\theta^2}{k^2}\left[\gamma_2 Y^2 - \frac{2\gamma_1}{3}\left(1+\frac{Y}{2}\right)\right]+\right.$$
$$\left.+\frac{2\theta^3}{k^4}\left[\frac{4}{3}\gamma_2^2 Y\left(1+\frac{Y}{2}\right)-2\left(\gamma_1^2+2\gamma_1\gamma_2\right)\left(1+\frac{Y}{2}\right)(1+Y)\right]\right\},$$
$$Y \equiv x\coth x,$$
$$\psi_0 = 3N\theta\left[x+\ln\left(1-e^{-2x}\right)\right],\ x=\frac{\hbar\omega}{2\theta},\ \omega=\sqrt{\frac{k}{m}} \tag{1}$$

where $U_0 = \frac{N}{2}u_0, u_0$ is the cohesive energy of an atom, N is the total atomic number of the metal, $\theta = k_{Bo}T$, k_{Bo} is the Boltzmann constant, T is the absolute temparature, $\hbar = \frac{h}{2\pi}$, h is the Planck constant, ω is the vibration frequency of atom at lattice point node, k, γ_1, γ_2 are parameters of the metal [38,39].

The cohesive energy u_0 the parameters k, γ_1, γ_2 and γ for cubic metals in the approximation of two coordination spheres have the forms as in [38,39]

The state equations for cubic metals are determined by [38,39,47]

$$Pv = -r_1\left(\frac{1}{6}\frac{\partial u_0}{\partial r_1}+\frac{\theta Y}{2k}\frac{\partial k}{\partial r_1}\right) \tag{2}$$

where $v = \frac{V}{N} = \frac{\sqrt{2}r_1^3}{2}$ is the volume of cubic unit cell per atom for face-centered cubic (FCC) lattice and $v = \frac{4r_1^3}{3\sqrt{3}}$ is that for body-centered cubic (BCC) lattice. If knowing the interaction potential between two atoms, we can find the solution of Eq. (2). This is the nearest neighbor distance between two atoms $r_{01}(P,0)$ at pressure P and temperature 0K. From that, we can determine the displacement of atom from the equilibrium position $y(P,T)$ and the nearest neighbor distance between two atoms $r_1(P,T)$ at pressure P and temperature T [38,39]

$$r_1(P,T) = r_{01}(P,0) + y(P,T) \tag{3}$$

The absolute stability limiting temperature for crystalline state T_s is determined by [38-45]

$$T_s = \frac{r_{1s}}{18k_B\gamma_G(P,T_s)}\left(\frac{\partial u_0}{\partial r_1}\right)_{T=T_s}+\left(\frac{\partial T}{\partial P}\right)_v P \tag{4}$$

where $r_{1s} = r_1(P,T_s)$ and $\gamma_G = -\frac{r_1 Y}{6k}\frac{\partial k}{\partial r_1}$ is the Gruneisen parameter of the metal. The melting temperature T_m of the metal is determined by [38-45]

$$T_m \approx T_s + \frac{r_{1m}-r_{1s}}{k_B\gamma_G(P,T_s)}\times$$
$$\times\left\{\frac{Pv(P,T_s)}{r_{1s}}+\frac{1}{18}\left[\left(\frac{\partial u_0}{\partial r_1}\right)_{T=T_s}+r_{1s}\left(\frac{\partial^2 u_0}{\partial r_1^2}\right)_{T=T_s}\right]\right\} \tag{5}$$

where $r_{1m} = r_1(P,T_m)$. $a_m = a(P,T_m)$.

The equilibrium vacancy concentration is given by [43,45,46]

$$n_v = \exp\left(\frac{u_0}{4\theta}\right) \tag{6}$$

Then, the melting temperature of defective metal is equal to [43,45,46]

$$T_m^R = T_m - \left(\frac{\partial T}{\partial n_v}\right)_{P,V} n_v(T_m) = T_m - \frac{T_m^2}{\frac{T_m}{4}\frac{\partial u_0}{\partial\theta}-\frac{u_0}{4k_{Bo}}} \tag{7}$$

The jump of volume at melting point of the metal is determined by [48]

$$\Delta v_m = \frac{\varepsilon\theta r_1^3}{\sqrt{2}k\langle u\rangle^2}\left(1+\frac{6\gamma^2\theta^2}{k^4}\right) \tag{8}$$

where ε is the metal constant and normally $\varepsilon = 0.01$ [48] and $\langle u\rangle = y$.

We determine the slope $\frac{\partial T_m}{\partial P}$ from the melting curve $T_m(P)$ of of defective metal calculated from Eq. (7). After that, we use the Clapeyron-Clausius equation to find the jump of enthalpy and entropy at melting point

$$\Delta H_m = \frac{T_m\Delta v_m}{\partial T_m/\partial P} \tag{9}$$

$$\Delta S_m = \frac{\Delta H_m}{T_m} \tag{10}$$

The isothermal compressibility, the thermal expansion coefficient and the heat capacity at constant volume and the Gruneisen parameter of cubic metals have the forms [38,39]

$$\chi_T = \frac{3\left(\frac{r_1}{r_{10}}\right)^3}{2P+\frac{r_1^2}{3V}\left(\frac{\partial^2\psi}{\partial r_1^2}\right)_T},$$
$$\left(\frac{\partial^2\psi}{\partial r_1^2}\right)_T = 3N\left\{\frac{1}{6}\frac{\partial^2 u_0}{\partial r_1^2}+\theta\left[\frac{Y}{2k}\frac{\partial^2 k}{\partial r_1^2}-\frac{1}{4k^2}\left(\frac{\partial k}{\partial r_1}\right)^2\left(Y+Z^2\right)\right]\right\},$$
$$Z \equiv \frac{x}{\sinh x} \tag{11}$$

$$\alpha = -\frac{k_B\chi_T}{3}\left(\frac{r_{10}}{r_1}\right)^2\frac{r_1}{3V}\left(\frac{\partial^2\psi}{\partial\theta\partial r_1}\right)$$

$$\frac{1}{3N}\frac{\partial^2\psi}{\partial\theta\partial r_1}=\frac{1}{2k}\frac{\partial k}{\partial r_1}Z^2+\frac{2\theta}{k^2}\left[\frac{\gamma_1}{3k}\frac{\partial k}{\partial r_1}\left(2+YZ^2\right)-\right.$$
$$\left.-\frac{1}{6}\frac{\partial\gamma_1}{\partial r_1}\left(4+Y+Z^2\right)-\left(\frac{2\gamma_2}{k}\frac{\partial k}{\partial r_1}-\frac{\partial\gamma_2}{\partial r_1}\right)YZ^2\right] \quad (12)$$

$$C_V=3Nk_{Bo}\left\{\begin{array}{l}Z^2+\frac{2\theta}{k^2}\left(2\gamma_2+\frac{\gamma_1}{3}\right)YZ^2+\\+\frac{\gamma_1}{3}\left(1+Z^2\right)-\gamma_2\left(Z^4+Y^2Z^2\right)\end{array}\right\} \quad (13)$$

$$\gamma_G=\frac{3\alpha V}{\chi_T C_V} \quad (14)$$

Therefore, from $r_1(P,T)$ we can find $V(P,T)$, $\chi_T(P,T)$, $\alpha_T(P,T)$, $C_V(P,T)$, và $\gamma_G(P,T)$. The Gruneisen parameter $\gamma_G(P,T)$ has the form [49]

$$\gamma_G(P,T)=\gamma_{G0}(0,T)\left[\frac{V(P,T)}{V_0(0,T)}\right]^q=$$
$$=\gamma_{G0}(0,T)\left[\frac{r_1(P,T)}{r_{01}(0,T)}\right]^{3q} \quad (15)$$

where q is the material constant and $q > 0$. The Gruneisen parameter is also defined by [38,39,47]

$$\gamma_G=-\frac{\partial\ln\omega_D}{\partial\ln V}=-\frac{\partial\ln\left(k_{Bo}T_D/\hbar\right)}{\partial\ln V} \quad (16)$$

where $\omega_D=\frac{k_{Bo}T_D}{\hbar}$ is the Debye frequency. The Debye temperature T_D is equal to [47,50]

$$T_D(P)=T_{D0}(0)\exp\left\{-\frac{\gamma_{G0}(0)}{q}\left[\left(\frac{V(P)}{V_0(0)}\right)^q-1\right]\right\},$$
$$T_{D0}(0)\approx\frac{4\hbar}{3k_{Bo}}\omega \quad (17)$$

3. Numerical results and discussions

For metals Ni. Pd and Pt, we use the Mie-Lennard-Jones (MLJ) *n-m* potential

$$\varphi(r)=\frac{D}{n-m}\left[m\left(\frac{r_0}{r}\right)^n-n\left(\frac{r_0}{r}\right)^m\right] \quad (18)$$

where r_0 is the distance between two atoms corresponding to minimum energy potential taking the value of $-D$, m, n are different numbers for different metals and are determined by empirical way on the basis of experimental data. The MLJ potential's parameters D, r_0, m, n for Ni. Pd and Pt are given in TABLE 1 [51,52]. Our calculated results are summarised in tables from TABLE 2 to TABLE 5 and illustrated in figures from Fig. 1 to Fig. 7.

TABLE 1

The MLJ potential's parameters for Ni, Pd and Pt [51,52]

Interaction	D/k_{Bo} (K)	r_0 (10^{-10} m)	m	n
Ni-Ni [51]	4325.16	2.4780	8.0	9.0
Pd-Pd [52]	7667.06	2.7432	2.89	11.85
Pt-Pt [52]	11366.40	2.7689	2.44	14.17

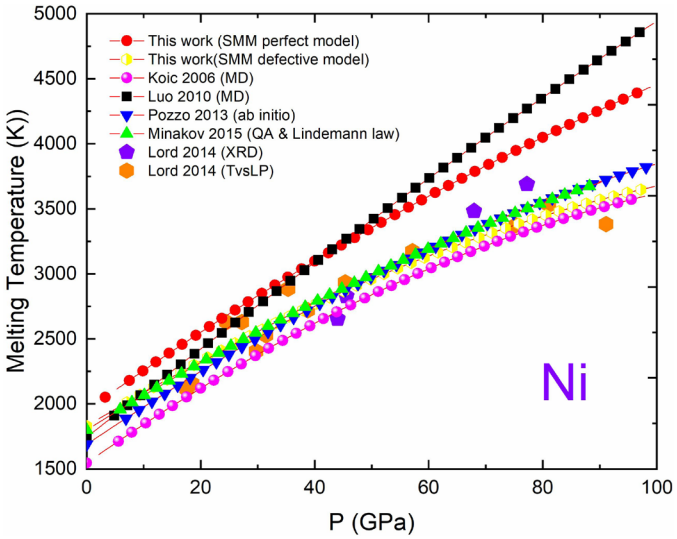

Fig. 1. $T_m(P)$ for Ni determined by SMM calculations, experimetal data [57] and other calculations [53-56]

In Fig. 1, the melting temperature $T_m(P)$ of Ni is calculated by SMM according to the model of perfect crystal from Eq. (5), SMM according to the model of defective crystal from Eq. (7), MD of Koci et al. (2006) [53] and Luo et al. (2010) [54], *ab initio* of Pozzo và Alfe (2013) [55], calculations in quasi-harmonic approximation (QA) and from Lindemann law of Minakov and Levashov (2015) [56], experiments from X-ray diffraction (XRD) and temperature versus laser power (TvsLP) plateau of Lord et al. (2014) [57].

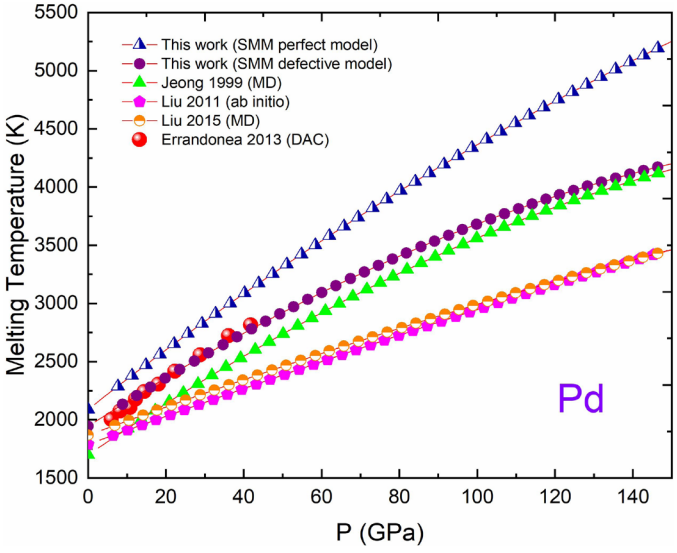

Fig. 2. $T_m(P)$ for of Pd determined by SMM calculations, experimetal data [61] and other calculations [58-60]

In Fig. 2, the melting temperature $T_m(P)$ Pd is calculated by SMM according to the model of perfect crystal from Eq. (5), SMM according to the model of defective crystal from Eq. (7), MD of Jeong và Chang (1999) [58] and Liu et al. (2015) [59], *ab initio* of Liu et al. (2011) [60] and và DAC experiments of Errandonea (2013) [61].

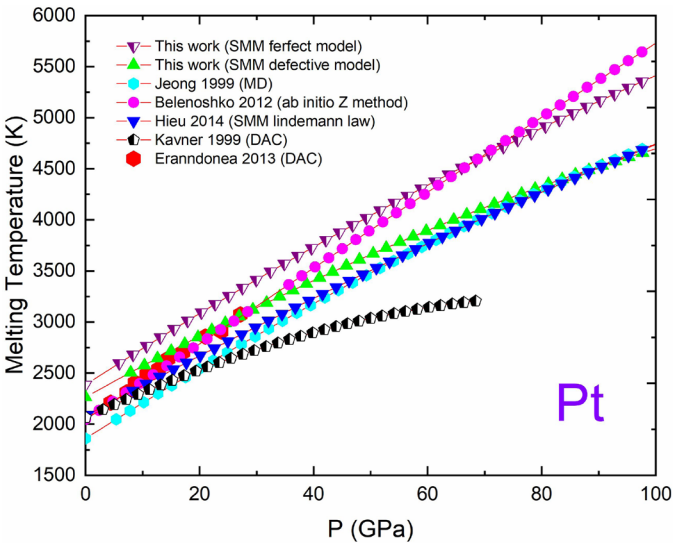

Fig. 3. $T_m(P)$ for Pt determined by SMM calculations, experimetal data [61,64] and other calculations [58,62,63]

In Fig. 3, the melting temperature $T_m(P)$ of Pt is calculated by SMM according to the model of perfect crystal from Eq. (5), SMM according to the model of defective crystal from Eq. (7), MD of Jeong and Chang (1999) [58], *ab initio* Z method of Belonoshko and Rosengren (2012) [62], calculations from Lindemann law of Hieu (2014)[63] and DAC experiments of Kavner and Jeanloz (1998) [64] and Errandonea (2013) [61].

Our SMM calculations of $T_m(P)$ according to the models of perfect and defective crystals are in good agreement with experiments from DAC and other calculations from MD, *ab initio*, Lindemann law and *ab initio* Z method. The higher the temperature, the larger the difference of the melting curve between the perfect metal and the defective metal. In the range from zero to 100 GPa, the maximum differences obtained for Pt, Ni and Pd are 13.3%, 17.5% and 20.18%, respctively. The maximum errors of the melting temperature between the SMM calculations according to the model of defective crystals and experiments for Pt, Ni and Pd are below 8.7%, 7.5% and 4.6%, respectively.

Our SMM calculations of $T_m(P)$, $(\partial T_m)/(\partial P)$, Δv_m, ΔH_m and ΔS_m for Pt, Ni and Pd are determined from Fig. 1, Fig. 2 and Fig. 3 and are summarized in TABLE 3, TABLE 4 and TABLE 5. When pressure increases from zero to 60 GPa, T_m increases from 2253 K to 3903.3 for Pt, from 1787 K to 3096 K for Ni and from 1925 K to 3548.2 for Pd; $(\partial T_m)/(\partial P)$ decreases from 31.12 K/GPa to 21.54 K/GPa for Pt, from 28 K/GPa to 18.2 K/GPa for Ni and from 33.88K/GPa to 17.66 K/GPa for Pd; Δv_m calculated from Eq. (8) decreases from 1.384×10^{-30} m^3 to 1.158×10^{-30} m^3 for Pt, from 1.232×10^{-30} m^3 to 0.909×10^{-30} m^3 for Ni and from 1.383×10^{-30} m^3 to 1.100×10^{-30} m^3 for Pd; ΔH_m calculated from Eq. (9) increases from 100.2 meV to 209.84 meV for Pt and from 78.56 meV to 221.01 meV for Pd; ΔS_m calculated from Eq. (10) changes from $0.0445k_B$ to $0.0537k_B$ for Pt, from $0.044k_B$ to $0.05k_B$ for Ni and $0.041k_B$ to $0.062k_B$ for Pd. The nearest neighbor distances between two atoms for metals, substitutional and interstitial alloys calculated from the SMM are in good agreement with experiments and other calculations in many previous papers [26-28,38-48]. The melting temperature for Pt, Ni, Pd calculated from the SMM also are in good agreement with experiments and other calculations in this paper. Therefore, we hope that the jumps of physical quantities obtained in this paper are highly reliable.

The nearest neighbor distance, the isothermal compressibility, the thermal expansion coefficient, the heat capacity at constant volume, the Gruneisen parameter and the Debye temperature of Ni at $T = 300$K and under pressure are summarized in Table 2. These quantities for Pt are illustrated on figures from Fig. 4 to Fig. 6. The isothermal compressibility, the thermal expansion coefficient, the heat capacity at constant volume and the Gruneisen parameter for metals under temperatures and pressure are in good agreement with experiments and other calculations (for example see [39]). Therefore, the Debye temperature of metals calculated from these quantities also are highly reliable.

TABLE 2

r_1 (10^{-10} m), χ_T (10^{-12} Pa^{-1}), α_T (10^{-5} K^{-1}), C_V (J/mol·K), γ_G and T_D (K) for Ni at $T = 300$K and under pressure

T (K)	P (GPa)	r_1	χ_T	α_T	C_V	γ_G	T_D
300 K	0	2.4661	7.0872	2.228	23.086	2.6092	399.20
	20	2.3983	3.8383	1.181	21.914	2.4745	493.68
	40	2.3564	2.7005	0.814	20.963	2.4035	561.88
	60	2.3257	2.1046	0.621	20.131	2.3569	617.58
	80	2.3012	1.7334	0.501	19.379	2.3228	665.64
1000 K	0	2.4910	9.0739	2.670	25.189	2.3066	364.13
	20	2.4131	4.3722	1.411	24.881	2.3281	454.16
	40	2.3674	2.9611	0.995	24.719	2.3037	517.84
	60	2.3345	2.2628	0.781	24.595	2.2802	569.11
	80	2.3087	1.8412	0.648	24.489	2.2601	612.92

According to Fig. 4a, 4b, 5a, 5b, 6a and 6b for Pt at the same temperature, quantities such as the nearest neighbor distance, the isothermal compressibility, the thermal expansion coefficient, the heat capacity at constant volume decrease and the Debye temperature increases with the increase of pressure. The decrease of the thermal expansion coefficient at higher temparatures is smaller than that at lower temparatures. For Pt at the lower temperatures (300K, 500K) when pressure increases, the Gruneisen parameter not significantly decreases. For Pt at the higher temperatures (from 1000K to 2000K) when pressure increases, the Gruneisen parameter nonlinearly increases. The increase of the Debye temperature is nonlinear.

For Pt at the same pressure, quantities such as the nearest neighbor distance, the isothermal compressibility, the thermal expansion coefficient, the heat capacity at constant volume in-

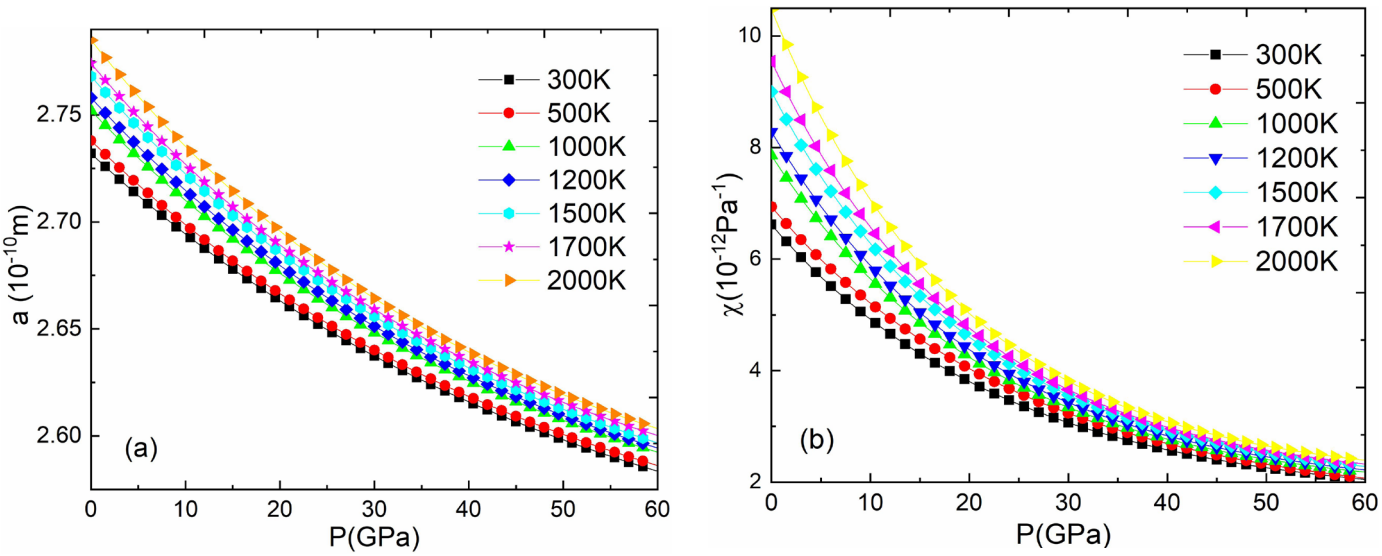

Fig. 4. (a) $r_1(P,T)$ and (b) $\chi_T(P,T)$ (b) for Pt

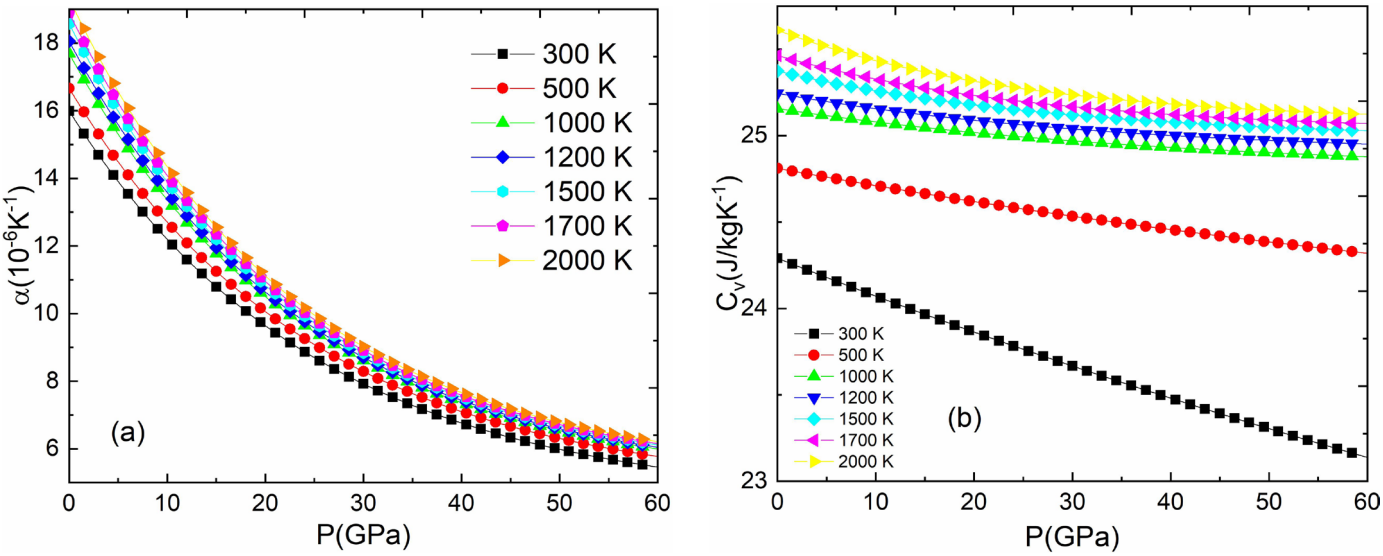

Fig. 5. (a) $\alpha_T(P,T)$ and $C_V(P,T)$ (b) for Pt

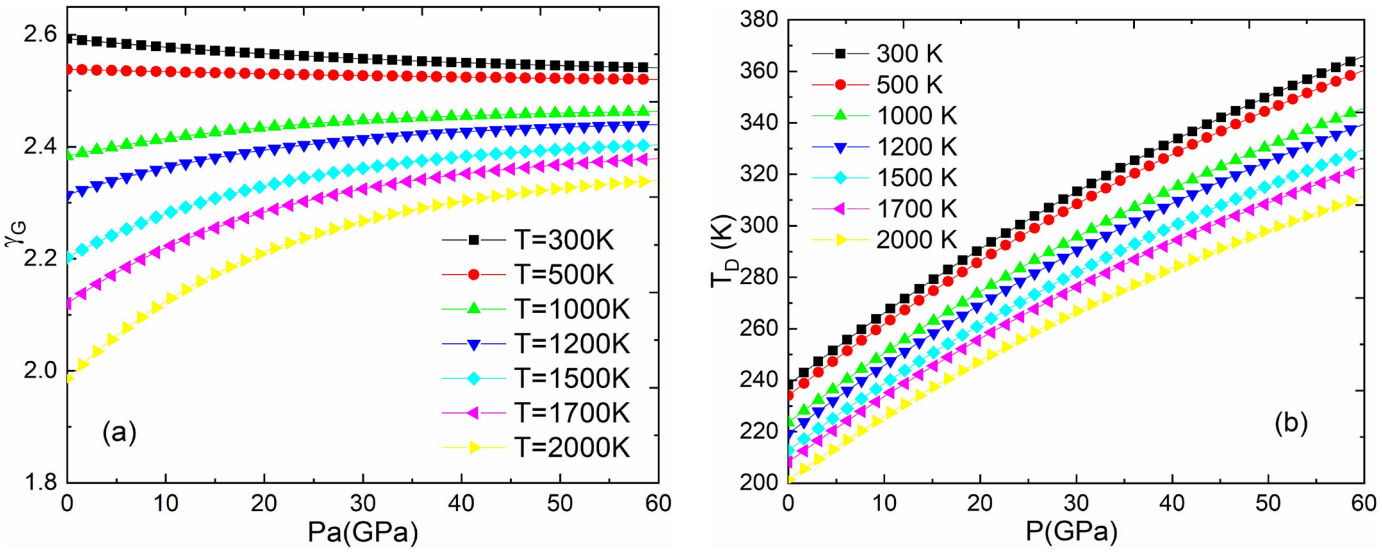

Fig. 6. (a) $\gamma_G(P,T)$ and (b) $T_D(P,T)$ for Pt

crease, the the Gruneisen parameter and the Debye temperature decrease with the increase of pressure.

According to tables from TABLE 3 to TABLE 5 and Fig. 7, the jump of volume at melting point for Pt, Ni and Pd nonlinearly decreases wth the increase of pressure. At the same pressure, the jump of volume at melting point for Pt is larger than that for Pd and the jump of volume at melting point for Pd is larger than that for Ni.

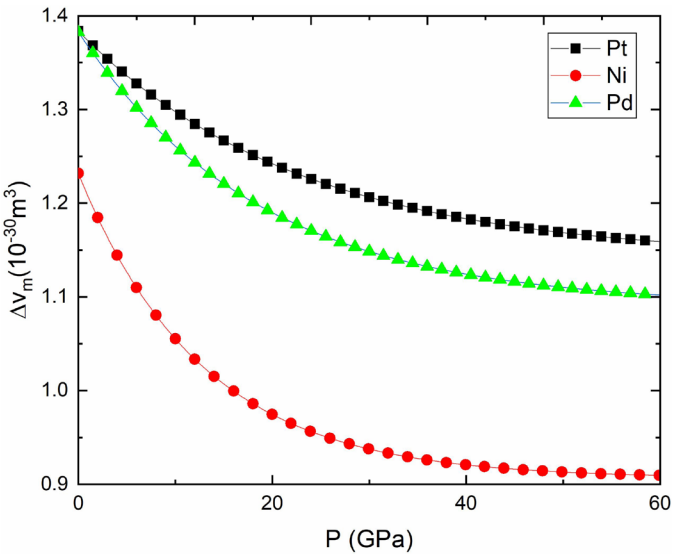

Fig. 7. $\Delta v_m(P)$ for Pt, Ni and Pd at $T = 300$ K

TABLE 3

T_m, $(\partial T_m)/(\partial P)$, Δv_m, ΔH_m and ΔS_m for Pt under pressure

***P* (GPa)**	**0**	**30**	**50**	**60**
T_m (K)	2253	3132.3	3666.6	3903.3
$(\partial T_m)/(\partial P)$ (K/GPa)	31.12	28.40	21.64	21.54
Δv_m (10^{-30} m^3)	1.384	1.206	1.17	1.158
ΔH_m (meV)	100.20	133.01	198.24	209.84
ΔS_m (k_B)	0.0445	0.0425	0.054	0.0537

TABLE 4

T_m, $(\partial T_m)/(\partial P)$, Δv_m, ΔH_m and ΔS_m for Ni under pressure

***P* (GPa)**	**0**	**30**	**50**	**60**
T_m (K)	1787	2312	2739	3096
$(\partial T_m)/(\partial P)$ (K/GPa)	28.0	25.2	21.0	18.2
Δv_m (10^{-30} m^3)	1.232	0.973	0.925	0.909
ΔS_m (k_B)	0.044	0.0386	0.044	0.05

TABLE 5

T_m, $(\partial T_m)/(\partial P)$, Δv_m, ΔH_m and ΔS_m for Pd under pressure

***P* (GPa)**	**0**	**30**	**50**	**60**
T_m (K)	1925	2857.4	3114.4	3548.2
$(\partial T_m)/(\partial P)$ (K/GPa)	33.88	23.92	17.68	17.66
Δv_m (10^{-30} m^3)	1.383	1.147	1.126	1.100
ΔH_m (meV)	78.56	137.02	198.35	221.01
ΔS_m (k_B)	0.041	0.046	0.064	0.062

4. Conclusion

We present the melting theory and the theory of Debye temperature for perfect and defective cubic metals under pressure mainly derived from the SMM. The SMM calculations of melting temperatures for Ni, Pd and Pt agree well with available experimental and theoretical data. Our SMM calculations of other physical quantities such as the jumps of volume, enthalpy and entropy at melting point, the isothermal compressibility, the thermal expansion coefficient, the heat capacity at constant volume, the Gruneisen parameter and the Debye temperature for Ni, Pd and Pt in the range from 300 to 2000K and from zero to 100 GPa are highly reliable.

REFERENCES

[1] D. Errandonea, B. Schwager, R. Ditz, C. Gessmann, R. Boehler, M. Ross, Systematics of transition-metal melting. Phys. Rev. B. **63** (13), 132104 (2001).
DOI: https://doi.org/10.1103/PhysRevB.63.132104

[2] S.N. Luo, T.J. Ahrens, Shock-induced superheating and melting curves of geophysically important minerals. Phys. Eart. Planet. Int. **143-144**, 369 (2004).
DOI: https://doi.org/10.1016/j.pepi.2003.04.001

[3] Q. An, S.N. Luo, L.B. Han, L. Zheng, O. Tschauner, Melting of Cu under hydrostatic and shock wave loading to high pressures. J. Phys: Cond. Matter. **20** (9), 8 pp (2008).
DOI: https://doi.org/10.1088/0953-8984/20/9/095220

[4] B.J. Jesson, P.A. Madden, Ab initio determination of the melting point of aluminum by thermodynamic integration. J. Chem. Phys. **113** (14), 5924 (2000).
DOI: https://doi.org/10.1063/1.1290701

[5] D. Errandonea, Improving the understanding of the melting behaviour of Mo, Ta, and W at extreme pressures. Phys. B: Cond. Matter. **357** (3-4), 356 (2005).
DOI: https://doi.org/10.1016/j.physb.2004.11.087

[6] L. Vočadlo, D. Alfè, Ab initio melting curve of the fcc phase of aluminum. Phys. Rev. B. **65** (21), 214105 (2002).
DOI: https://doi.org/10.1103/PhysRevB.65.214105

[7] C.M. Liu, X.R. Chen, C. Xu, L.C. Cai, F.Q. Jing, Melting curves and entropy of fusion of body-centered cubic tungsten under pressure. J. Appl. Phys. **112** (1), 013518 (2012).
DOI: https://doi.org/10.1063/1.4733947

[8] H.M. Strong, F.P. Bundy, Fusion curves of four group VII metals to 100 000 atm. Phys. Rev. **115**, 278 (1959).
DOI: https://doi.org/10.1103/PhysRev.115.278

[9] H.M. Strong, Melting and other phase transformations at high pressure. In Progress in very high pressure research, in: F.P. Bundy et al. (Eds.), John Wiley and Sons, New York (1961).

[10] D. Errandonea, B. Schwager, R. Ditz, C. Gessmann, R. Boehler, M. Ross, Systematics of transition-metal melting. Phys. Rev. B. **63**, 132104, 1 (2001).
DOI: https://doi.org/10.1103/PhysRevB.63.132104

[11] P. Lazor, PhD Thesis, Phase diagrams, elasticity and thermodynamics of Ni, Co and Fe under high pressure, Uppsala University, Sweden (1994).

[12] Z. Wang, P. Lazor, S.K. Saxena, A simpled modeo for assessing the high pressure melting of metals: nickel, aluminium and platinum. Phys. B, **293**, 408 (2001).
DOI: https://doi.org/10.1016/S0921-4526(00)00542-1

[13] A.K. McMahan, R.C. Albers, Insulating nickel at a pressure of 34 Tpa (340 Mbar). Phys. Rev. Lett. **49**, 1198 (1982).
DOI: https://doi.org/10.1103/PhysRevLett.49.1198

[14] D.A. Young, Phase diagrams of the elements, Berkeley, University of California Press, California (1991).

[15] B. Chen, D. Penwell, MB. Bruger, The compressibility of nanocrystalline nickel. Solid State Commun. **115** (4), 191 (2000).
DOI: https://doi.org/10.1016/S0038-1098(00)00160-5

[16] H.K. Mao, P.M. Bell, J.Shaner, D. Steinberg (1979), A System of pressure calibration for the range 0.05-1.0 Mbar based on shock wave equations of state for Cu, Mo, Pd, and Ag. In: K.D. Timmerhaus, M.S Barber (Eds.), high pressure science and technology. Springer, Boston, MA (1977).

[17] H.K. Mao, P.M. Bell, J. Shaner, D. Steinberg, Specific volume measurements of Cu, Mo, Pd and Ag and calibration of the ruby R fluorescence pressure gauge from 0.06 to 1 Mbar. J. Appl. Phys. **49**, 3276 (1978). DOI: https://doi.org/10.1063/1.325277

[18] P. Soderlind, O. Eriksson, B. Johansson, J.M. Wills, Theory of elastic constants of cubic transition metals and alloys. Phys. Rev. B. **48**, 5844 (1993). DOI: https://doi.org/10.1103/PhysRevB.48.5844

[19] E.A. Perez-Albuerne, K.F. Forsgren, H.G. Drickamer, Apparatus for X-ray measurements at very high pressure. Rev. Sci. Instrum. **35**, 29 (1964). DOI: https://doi.org/10.1063/1.1718703

[20] N. Singh, Structural phase transformation of Cu, Pd and Au using transition metal pair potential. Phys. B. **269**, 211 (1999).
DOI: https://doi.org/10.1016/S0921-4526(98)00660-7

[21] A. Migault, J.P. Jamain, J. Jacquesson, Fusion curves at high pressure and Gruneisen parameter of metals, In 7 Int. AIRAPT conf. high pressure science and technology, Le Creusot (France), **2**, 938 (1979).

[22] H. Schlosser, P. Vinet, J. Ferrante, Pressure dependence of the melting temperature of metals. Phys. Rev. B. **40**, 5929 (1989).
DOI: https://doi.org/10.1103/physrevb.40.5929

[23] J.W. Jeong, K.J. Chang, Molecular-dynamics simulation for the shock Hugoniot meltings of Cu, Pd and Pt. J. Phys.: Cond. Matter. **11**, 3799 (1999). DOI: https://doi.org/10.1103/PhysRevB.59.329

[24] L.F. Vereshchagin, N.S. Fateeva, Melting temperatures of refractory metals at high pressures. High Temp.-High Pres. **9**, 619 (1977).

[25] A. Kavner, R. Jeanloz, High-pressure melting curve of platinum. J. Appl. Phys. **83**, 7553 (1998).
DOI: https://doi.org/10.1063/1.367520

[26] N.Q.Hoc, B.D.Tinh and N.D.Hien, Influence of temperature and pressure on the electrical resistivity of gold and copper up to 1350K and 100 GPa. Mater. Res. Bull. **128**, 110874 (2020).
DOI: https://doi.org/10.1016/j.materresbull.2020.110874G

[27] N.Q. Hoc, B.D. Tinh, N.D. Hien, Stress – strain curve of FCC interstitial alloy AuSi under pressure. Rom. J. Phys. **65**, 608 (2020).

[28] N.Q. Hoc, B.D. Tinh, G. Coman, N.D. Hien, On the melting of alloys FeX (X = Ni, Ta, Nb, Cr) under pressure up to 5 GPa. J. Phys. Soc. Jpn. **89**, 114602 (2020).
DOI: https://doi.org/10.7566/JPSJ.89.114602

[29] N.T. Dung, Inffluence of impurity concentration, atomic number, temperature and tempering time on microstructure and phase transformation of $Ni_{1-x}Fe_x$(x = 0,1, 0,3, 0,5) nanoparticles. Mod. Phys. Lett. B **32**, 1850208 (2020).
DOI: https://doi.org/10.1142/S0217984918502044

[30] T.Q. Tuan, N.T. Dung, Effet of heating rate, cupper impurity concentration, atomic numbedr, temperature, annealing time on structure, crystalization temperature and crystallization process of $Ni1\text{-}xCu_x$ (x = 0,1, 0,3, 0,5, 0,7). Int. J. Mod. Phys. B **32**, 18300009 (2018). DOI: https://doi.org/10.1142/S0217979218300098

[31] N.T. Dung, P.L. Kien, N.T. Phuong, Simulation on the factors affecting crystallization process of FeNi alloy by molecular dynamics. ACS Omega **4**, 14605 (2019).
DOI: https://doi.org/10.1021/acsomega.9b02050

[32] N.T. Dung, N.C. Cuong, D.Q. Van, Study on the effect of doping on lattice constant and electronic structure of bulk AuCu by the density functional theory. J. Multiscale Mod. **11**, 2030001 (2020).
DOI: https://doi.org/10.1142/S1756973720300014

[33] N.T. Dung, N.T. Phuong, Molecular dynamics study on factors influencing the structure, phase transition and crystallization process of NiCu6912 nanoparticle. Mater. Chem. Phys. **250**, 123075 (2020). DOI: https://doi.org/10.1016/j.jallcom.2019.152133

[34] C.L. Van, D.Q. Van, N.T. Dung, *Ab initio* calculations on the structural and electronic properties of AgAu alloys. ACS Omega **5**, 31391 (2020). DOI: https://doi.org/10.1021/acsomega.0c04941

[35] N.T. Dung, C.L. Van, S. Talu, The structure and crystalizing process of NiCu alloy: A molecular dynamic simulatiom method. J. Compos. Sci. **5**, 18 (2021).
DOI: https://doi.org/10.3390/jcs5010018

[36] N.T. Dung, Z-axis deformation method to investigate of system size, structural phase transition on mechanical properties of bulk nickel. Mater. Chem. Phys. **252**, 123275 (2020).
DOI: https://doi.org/10.1016/j.matchemphys.2020.123275

[37] T.Q. Tuan, N.T. Dung, S. Talu, Study on the influence of factors on the structural and mechanical properties of amorphous aluminium by molecular dynamics method. Adv. Mater. Sci. Eng. **1**, 5564644 (2021). DOI: https://doi.org/10.1155/2021/5564644

[38] N. Tang, V.V. Hung, Investigation of the thermodynamic properties of anharmonic crystals by the momentum method. Phys. Stat. Sol. (b), **149**, 511 (1988); **161**, 165 (1990); **162**, 371 (1990); **162**, 379 (1990).
DOI: https://doi.org/10.1002/pssb.2221490212;
DOI: https://doi.org/10.1002/pssb.2221610115;
DOI: https://doi.org/10.1002/pssb.2221620206;
DOI: https://doi.org/10.1002/pssb.2221620207

[39] V.V. Hung, Statistical moment method in studying elastic and thermodynamic properties of crystals, HNUE Publishing House (2009).

[40] L.T.C. Tuyen, N.Q. Hoc, B.D. Tinh, D.Q. Vinh, T.D. Cuong, Study on the melting of interstitial alloys FeH and FeC with BCC structure under pressure. Chin. J. Phys. **59**, 1, (2019).
DOI: https://doi.org/10.1155/2018/5251741

[41] T.D. Cuong, N.Q. Hoc, P.D. Anh, Application of the Statistical Moment Method to Melting Properties of Ternary Alloys with FCC Structure. J. Appl. Phys. **125**, 215112 (2019). DOI: https://doi.org/10.1063/1.5089228

[42] T.D. Cuong, G. Coman, N.Q. Hoc, N.T. Hoa, D.Q. Vinh, The melting temperature of BCC perfect ternary alloy FeCrC under pressure. IOP Conf. Ser.: Mater. Sci. Eng. **595**, 012018 (2019). DOI: https://doi.org/10.1088/1757-899X/595/1/012018

[43] V.V. Hung, D.T. Hai, L.T.T. Binh, Melting curve of metals with defect: Presure dependence. Comp. Mat. Sci. **79**, 789 (2013). DOI: https://doi.org/10.1016/j.commatsci.2013.07.042

[44] N.Q. Hoc, L.H. Viet, N.T. Dung, On the melting of defective FCC interstitial alloy FeC under pressure up to 100 GPa. J. Electron. Mater. **49** (2), 910 (2020). DOI: https://doi.org/10.1007/s11664-019-07829-9

[45] N.Q. Hoc, T.D. Cuong, B.D. Tinh, L.H. Viet, Study on the melting of defective interstitial alloys TaSi and WSi with BCC structure. J. Korean Phys. Soc. **71** (8), 801 (2019). DOI: https://doi.org/10.3938/jkps.74.801

[46] N.Q. Hoc, T.D. Cuong, B.D. Tinh, L.H. Viet, High-pressure melting curves of FCC metals Ni, Pd and Pt with defects, Mod. Phys. Lett. B, **33** (25), 1950300 (2019). DOI: https://doi.org/10.1142/S0217984919503007

[47] N.Q. Hoc, N.D. Hien, N.T. Dung, C.L. Van, S. Talu, Study on the malting temperature, the jumps of volume, entahalpy and entropy and the Debye temperature for the BCC defective and perfectinterstitial alloys WSi under pressure. J. Compos. Sci. **5**, 153 (2021). DOI: https://doi.org/10.3390/jcs5060153 https://doi.org/10.1016/j.matchemphys.2020.123275

[48] V.V. Hung, Investigation of the change in volume, entropy and specific heat for metals on melting. Proc. the 22nd National Conference of Theoretical Physics, Do Son (Vietnam), 3-5.8.1997, 199.

[49] M.J. Graf, C.W. Greeff, J.C. Boettger, High-Pressure Debye-Waller and Grüneisen parameters of gold and copper. AIP Conf. Proc. **706** (1), 65 (2004). DOI: https://doi.org/10.1063/1.1780185

[50] L.A. Girifalco, Statistical physics of materials, John Wiley and Sons, New York (1973).

[51] M.N. Magomedov, On calculating the Debye temperature and the Gruneisen parameter. Zhur. Fiz. Khim. **61** (4), 1003, (1987) (in Russian).

[52] M.N. Magomedov, The calculation of the parameters of the Mie-Lennard-Jones potential. High Temp. **44** (4), 513 (2006). DOI: https://doi.org/10.1007/s10740-006-0064-5

[53] L. Koci, E.M. Bringa, D.S. Ivanov, J. Hawreliak, J. McNaney, A. Higginbotham, R. Ahuja, Simulation of shock-induced melting of Ni using molecular dynamics coupled to a two-temperature model. Phys. Rev. B **74** (1), 012101 (2006). DOI: https://doi.org/10.1103/PhysRevB.74.012101

[54] F. Luo, X.R. Chen, L.C. Cai, G.F. Ji, Solid-liquid interfacial energy and melting properties of nickel under pressure from molecular dynamics. J. Chem. Eng. Data, **55** (11), 5149 (2010). DOI: https://doi.org/10.1021/je1007058

[55] M. Pozzo, D. Alfe, Melting curve of face-centeredcubic nickel from first principles calculations. Phys. Rev. B **88** (2), 024111 (2013). DOI: https://doi.org/10.1103/PhysRevB.88.024111

[56] D.V. Minakov, P.R. Levashov, Melting curves of metals with excited electrons in the quasiharmonic approximation. Phys. Rev. B **92** (2), 224102 (2015). DOI: https://doi.org/10.1103/PhysRevB.92.224102

[57] O.T. Lord, I.G. Wood, D.P. Dobson, L. Vocadlo, W. Wang, A.R. Thomson, E.T.H. Wann, G. Morard, M. Mezouar, M.J. Walter, The melting curve of Ni to 1 Mbar. Earth Plan. Sci. Let. **408**, 226 (2014). DOI: https://doi.org/10.1016/j.epsl.2014.09.046

[58] J.W. Jeong, K.J. Chang, Molecular-dynamics simulations for the shock Hugoniot melting of Cu, Pd and Pt. J. Phys.: Cond. Matter, **11** (19), 3799 (1999). DOI: https://doi.org/10.1088/0953-8984/11/19/302

[59] Z.L. Liu, X.L. Zhang, L.C. Cai, Shock melting method to determine melting curve by molecular dynamics: Cu, Pd and Al. J. Chem. Phys. **143** (11), 114101 (2015). DOI: https://doi.org/10.1063/1.4930974

[60] Z.L. Liu, J.H. Yang, L.C. Cai, F.Q. Jing, D. Alfe, Structurtal and thermodynamic properties of compressed palladium: Ab initio and molecular dynamics study. Phys. Rev. B **83** (14), 144113 (2011). DOI: https://doi.org/10.1103/PhysRevB.83.144113

[61] D. Errandonea, High-pressure melting curves of the transition metals Cu, Ni, Pd and Pt. Phys. Rev. B **87** (5), 054108 (2013). DOI: https://doi.org/10.1103/PhysRevB.87.054108

[62] A.B. Belonoshko, A. Rosengren, High-pressure melting curve of platinum from ab initio Z method. Phys. Rev. B **85** (17), 174104 (2012). DOI: https://doi.org/10.1103/PhysRevB.85.174104

[63] H.K. Hieu, Systematic prediction of high-pressure melting curves of transition metals. J. Appl. Phys. **116** (16), 163505 (2014). DOI: https://doi.org/10.1063/1.4899511

[64] A. Kavner, R. Jeanloz, High-pressure melting curve of platinum. J. Appl. Phys. **83** (12), 7553 (1998). DOI: https://doi.org/10.1063/1.367520